JTTEE5 14:258-263
DOI: 10.1361/10599630523836
1059-9630/$19.00 © ASM International

Peer Reviewed

Long Crack Behavior in a Thermal Barrier Coating Upon Thermal Shock Loading

Y. Liu, C. Persson, S. Melin, and J. Wigren

(Submitted September 15, 2003; in revised form November 18, 2003)

The behavior of macroscopic long cracks in the ceramic top coat of a thermal barrier coating (TBC) system subjected to thermal shock loading and the influence of the cracks on the coating durability were investigated experimentally and numerically. Thermal shock testing was conducted until coating failure. Comparisons were made with coating samples without macroscopic cracks. The experimental results revealed that the presence of macroscopic cracks reduces the life of the TBC. The finite-element method, with a fracture mechanics approach, was applied to analyze preexisting long cracks, and the calculations correlate well with the experimental findings. It was found that the life of the coating is reduced with crack length as well as with maximum cycle temperature. It was also found that the stress-intensity factors for long cracks are initially high and decrease with the number of temperature cycles, which indicates that rapid crack growth occurs during the first number of cycles.

Keywords finite-element method, long cracks, thermal barrier coatings, thermal shock tests

1. Introduction

Plasma-sprayed thermal barrier coating (TBC) systems are widely used to protect gas turbine components from their hash and severe thermal environments. Typical TBC systems comprise an insulating ceramic top coat, a structural load carrying the superalloy substrate, and a bond coat containing aluminum between the substrate and the top coat, providing oxidation protection. The interface between the bond coat and the top coat might also contain a thermally grown oxide (TGO), predominantly aluminum oxide. The plasma spray process imparts a rough and wavy interface to the bond coat and a porous structure, containing a substantial number of cracks, to the top coat.

TBC systems typically fail by spallation, predominantly at the interface region, as reported by DeMasi et al. (Ref 1) and Meier et al. (Ref 2). Due to its low fracture resistance, crack initiation mostly occurs within the ceramic top coat, with subsequent crack propagation close to the interface (Ref 3-5). The crack propagation is influenced by factors such as the presence of TGO and the undulation of the interface (Ref 6).

Studies of TBCs during thermal cycling indicate that crack initiation occurs at a relatively early stage (Ref 3). Due to the sensitivity of the resulting fracture toughness of TBCs to the deposition process, as well as the difficulty in testing the coatings, the overall toughness domain of the TBC system is minimally encompassed, as shown by Evans et al. (Ref 7). They investigated the sensitivity to fracture from cracks of lengths <100 μm up to a few millimeters and found the sensitivity to increase with crack length. The overall mode I toughness was found to vary between 0.1 and 1 MPa√m, and the mode II toughness between 3 and 5 MPa√m. Qian et al. (Ref 3) investigated the tensile toughness of a TBC with a centrally situated crack of length a = 2.5 mm in the top coat. In contrast to Evans et al. (Ref 7), Qian et al. (Ref 3) they found a low mode I toughness of 0.23 MPa√m.

The behavior of preexisting short cracks, with crack lengths in the range 10 to 360 μm, situated in the ceramic top coat of a plasma-sprayed TBC system and subjected to thermal shock loading, has previously been investigated (Ref 8, 9). The studies showed that the position of a crack in the coating as well as the undulation of the interface, the TGO, and the friction between the crack surfaces influence the fracture behavior.

The current study focused on the behavior of macroscopic cracks that are present in the top coat close to the interface. Thermal shock experiments were performed on as-sprayed samples holding prefabricated cracks and finite-element (FE) simulations of the experiments are carried out. Comparisons were made with the results of Liu et al. (Ref 9) in which an investigation of as-sprayed samples, which were assumed to contain inherent microcracks, was performed. The influence on the risk of fracture from interface undulation, temperature range, and crack face friction was investigated.

2. Experimental Procedure

Through air plasma spraying, a NiCoCrAlY bond coat was deposited on a nickel-base superalloy Hastelloy X cylindrical sample according to the standard procedures of Volvo, as described in the article by Liu et al. (Ref 10). The diameter of the cylinder was 25.4 mm, and the height was 6.0 mm. Figure 1 shows the microstructure of the sample in the region close to the interface, and illustrates the undulation of the interface and the porosity of the top coat. The thicknesses of the top coat and the bond coat were about 0.50 and 0.09 mm, respectively.

Two different types of samples were compared. One set of eight samples was tested as-sprayed (Ref 10). The second set,

Y. Liu and **C. Persson**, Division of Materials Engineering, and **S. Melin,** Division of Solid Mechanics, Department of Mechanical Engineering, Lund University, SE-22100, Lund, Sweden; and **J. Wigren**, Volvo Aero Corporation, SE-46181, Trollhättan, Sweden. Contact e-mail: yan.liu@telia.com.

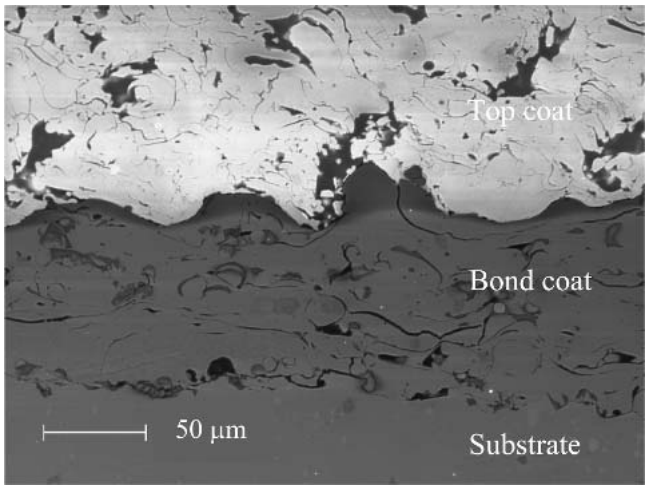

Fig. 1 Scanning electron micrograph of the TBC system

likewise containing eight samples, was prepared with prefabricated cracks. A paintbrush 2 mm in width was used to apply an antibond strip on top of the bond coat along the diameter of the cylindrical surface before the top coat was sprayed. An interface crack resulting from this procedure is shown in Fig. 2. To be noted is a local thinning of the top coat occurring at the center of the top surface. This apparent material shrinkage of the top coat is due to the residual stresses that evolved in the top coat during cooling after the spraying process. But it was not be modeled due to the relatively small volumetric change and for simplification as well.

Thermal shock-life tests of the two groups of samples mentioned above were conducted in a thermal shock test rig. The samples were subjected to a series of heating and cooling cycles of a total duration of 150 s, with the same heating and cooling times (Ref 10). A video camera system was attached in front of the coating surface to monitor the coating during testing. The tests were performed until coating failure. The coating life was determined as the number of cycles to failure, which was defined to occur when >10% of the coating area had spalled from the top surface.

3. Finite-Element Modeling

Finite-element analyses were performed using the general-purpose FE code Abaqus (Ref 11). The three-dimensional cylindrical problem was reduced to a two-dimensional geometry by considering the cross section of the cylindrical sample only. The model geometry is depicted in Fig. 3. Due to symmetry, only half of the cross section is modeled. The *Y*-axis is the axis of symmetry. The width *L* equals half of the sample diameter, and *H* is the height of the sample. A stationary, horizontal, centrally situated crack of half length ($a_i + a_{ii}$) was introduced at the distance $d = 10$ μm above the interface. The length a_i was chosen as 1 mm, modeling the crack introduced by the antibond coat treatment of the samples. The distance a_{ii} was varied between 5 and 180 μm to investigate the influence of the undulation of the interface on the crack tip region. A mean size of 0.15 ± 0.02 mm,

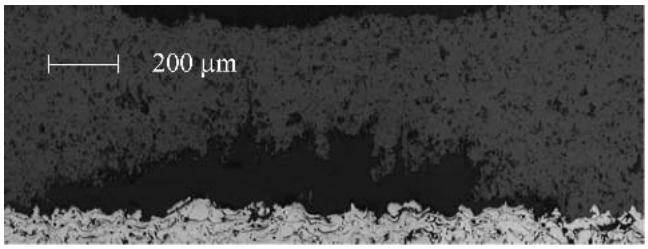

Fig. 2 Antibond strip-induced interface crack

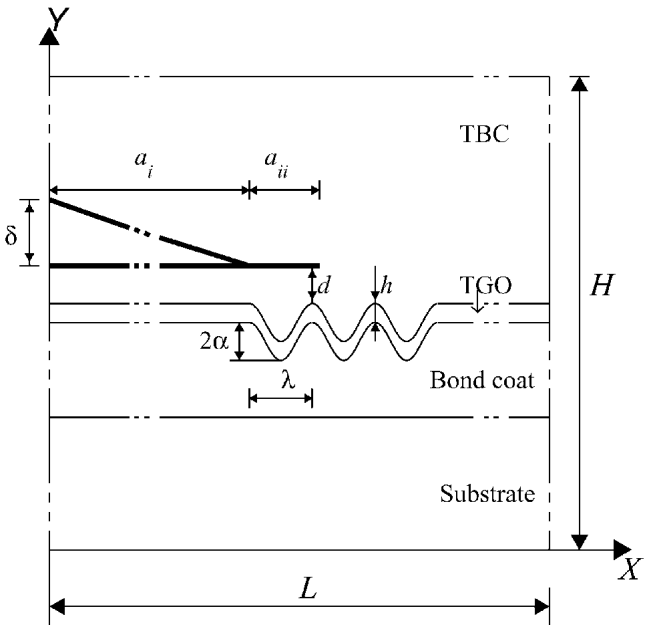

Fig. 3 Schematic geometry of the TBC system in the FE model

as estimated from micrographs (Fig. 2), was chosen for the initial crack opening δ at the center of the sample.

The profile of the bond coat roughness was taken to be sinusoidal with wavelength λ = 110 μm and amplitude 2α = 25 μm, as estimated from experiments (Ref 10). The wavy interface extends for three wavelengths, which is long enough compared with the length of the single microcrack of the top coat in the region of the crack tip position, and thereafter was smoothened into a plane surface to simplify the model. No oxide layer was included in the model due to the short duration of the thermal shock tests, during which no oxide growth was expected.

A comparison with as-sprayed samples without macroscopic cracks was also made. These samples were assumed to contain inherent microcracks. In the FE model, $a_i = 0$, thus modeling a line-shaped crack with the half-crack length a_{ii} (Ref 9).

The numerical calculations were performed in two steps: a thermal analysis followed by a mechanical analysis, with the calculated node temperatures from the thermal analysis used as input to the mechanical analysis (Ref 9, 10).

In the thermal analysis, cyclic thermal loading of the system is simulated through the adjustment of the heat flux through the sample (Ref 10) to model the experimental temperature load. Maximum temperatures at the center of the top coat surface (*X* =

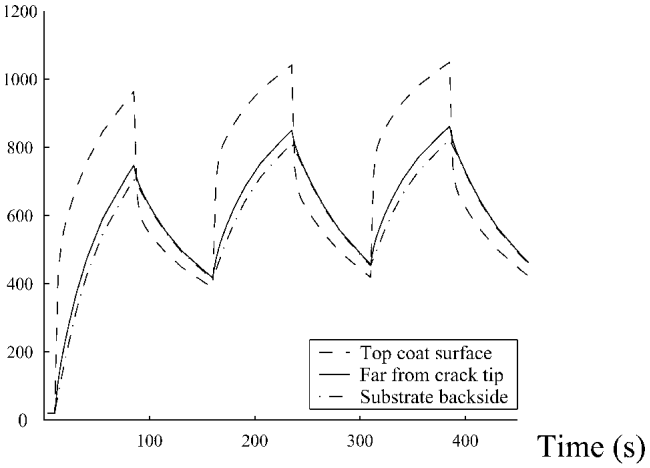

Fig. 4 Simulated temperature variation during the three first loading cycles

0, Y = H) were chosen: $T1$ = 1020 °C; $T2$ = 1140 °C; and $T3$ = 1240 °C. At the bottom surface of the sample, the temperature was in the interval between 430 and 450 °C. A typical example of the simulated temperature variation during the three first loading cycles is shown in Fig. 4.

In the mechanical analysis, eight-node generalized plane strain elements were used. Contact elements were introduced between the crack surfaces to avoid overlap and to provide the possibility of introducing Coulomb friction between the crack surfaces whenever they were in contact. The coefficient of friction was chosen as either 0 or 0.5. The square root singularity at the crack tip was modeled by focusing the mesh at the crack tip (Ref 12). The mode I and mode II stress intensity factors at the crack tip, K_I and K_{II}, were continuously calculated from the displacements at the nodes closest to the crack tip during the mechanical analysis. The simulations were performed until steady state was reached, with steady state defined as prevailing when the maximum and minimum values of both K_I and K_{II} varied <0.1% between consecutive load cycles.

The material parameters were temperature-dependent, and their values at 700 °C are given in Table 1. Both the TBC and the oxide layer were assumed to be elastic, whereas the bond coat and the substrate were modeled as being elastic-viscoplastic, obeying the von Mises yield criterion for perfect plasticity and the Norton creep law.

4. Results and Discussion

4.1 Experimental Results

The experimental results for the different sample sets are summarized in Table 2. The life of each individual sample was judged from the video recordings, and the average life was calculated as a mean of the individual lives.

Reviewing video recordings of the tests, the following observations were made. For antibond strip samples, the first sign of degradation was a bright elliptical region lying adjacent to the antibond strip. This bright spot indicated a separation between

Table 1 Material properties for different layers at 700°C (Ref 1, 10)

Layers	Ceramic coat	Al_2O_3	Bond coat	Substrate
E, GPa	17	345	103	150
Poisson's ratio	0.20	0.32	0.27	0.30
Yield stress, MPa	…	…	95	270
CTE, $\times 10^{-6}$/°C)(a)	11.00	7.79	15.00	15.00
Creep behavior(b)	…	…	A = 2.04e-34	A = 3.18e-56
		…	B = 3.35	B = 6.00

(a) CTE, coefficient of thermal expansion. (b) Defined by the relation $\dot{\varepsilon} = A\sigma^B$, where $\dot{\varepsilon}$ is the strain rate in unit of s^{-1}, A is the creep coefficient in units of $(MPa)^{-B}s^{-1}$, σ is the effective von Mises stress in MPa and B is the dimensionless creep exponent.

Table 2 Results of thermal shock tests

Samples	T_{max}, °C	Cycles to failure(a)	Failure mode
As-sprayed	1070	3300 ± 1276	Edge/central spallation
As-sprayed	1230	346 ± 183	Edge/central spallation
Anti-bond strip	1050	848 ± 382	Vast spallation
Anti-bond strip	1250	316 ± 152	Vast spallation

(a) Mean value ± SD

the bond coat and the top coat, and would be the result of crack propagation along the interface, initiating from the edge of the antibond strip. The size of this region grew rapidly, with delamination covering half of the sample in just a small number of thermal cycles. This region grew eventually, leading to spallation and final failure.

The failure lives of the as-sprayed samples were longer than those of the antibond samples, even if the difference became less obvious at higher temperatures. First, chipping (i.e., the spallation of small parts of the ceramic top coats) was observed in the central region of the sample, which is the hottest part during testing. This was, however, not the mechanism that led to final coating failure. Shortly before the lifetime was reached, a bright region (i.e., delamination) was seen at the edge of the sample. This region grew rapidly, and spallation occurred, leading to final failure.

From Table 2 it can be seen that the life of the sample decreases as the maximum cycle temperature increases. It is also seen that a macroscopic crack reduces the life of the sample compared with the as-sprayed case. The difference is, though, not so pronounced at the higher temperature.

It should be remembered that the failure modes differ between the samples. An initial degradation of the anti-bond-coated samples seemed to occur very rapidly, during a few load cycles only, followed by a slower degradation; whereas, the degradation of the as-sprayed samples increased gradually over time.

4.2 Numerical Results

Figure 5 shows the numerical results for a sample containing a central antibond strip crack that had been subjected to a maximum temperature of T = 1020 °C at the sample center. Due to the thermal insulation offered by the crack, the temperature profile

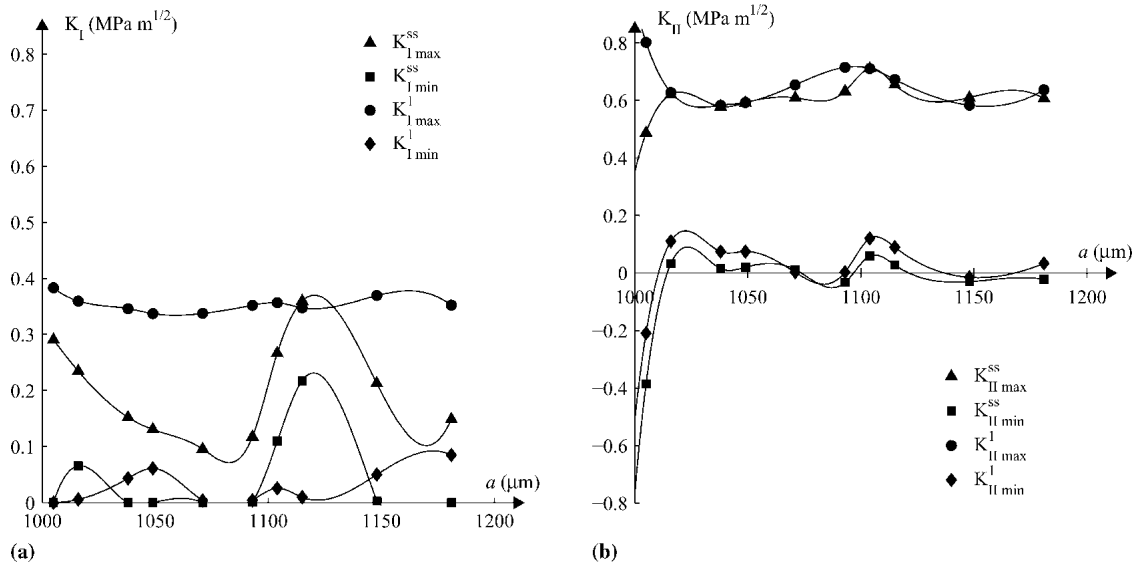

Fig. 5 Maximum and minimum values of (a) K_I and (b) K_{II} during the first load cycle and at steady state for antibond strip cracks. The friction coefficient between the crack surfaces is 0.5.

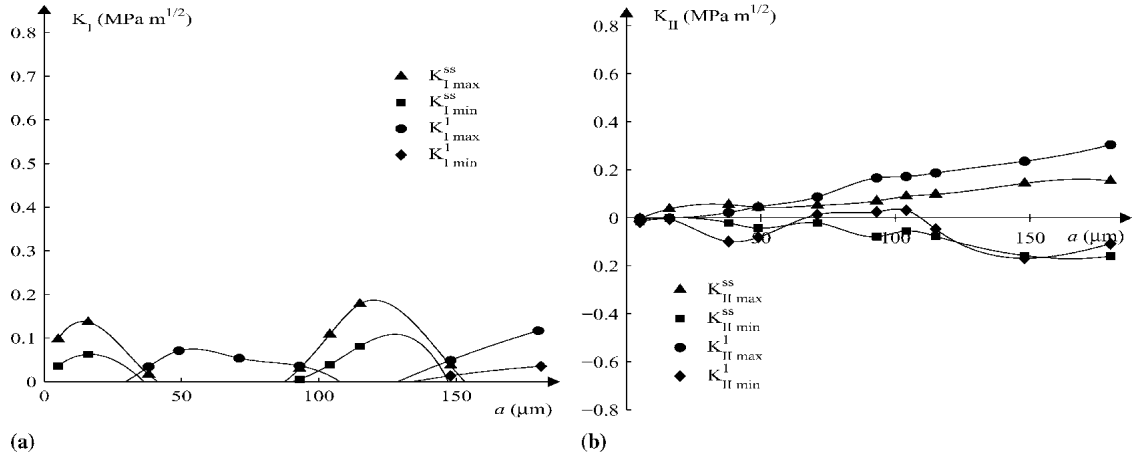

Fig. 6 Maximum and minimum values of (a) K_I and (b) K_{II} during the first load cycle and at steady state for short cracks. The friction coefficient between the crack surfaces is 0.5.

along the top coat surface varied. Imposing a temperature of T = 1020 °C at position ($X = 0$, $Y = H$) resulted in a temperature of only T = 930 °C at position ($X = a_i$, $Y = H$), which is a temperature drop of about 90 °C. This is, however, consistent with the experimental observation that the hottest part of the sample is at the center.

The maximum and minimum values of K_I at the tip during the first load cycle (K^1_{Imax} and K^1_{Imin}) and at steady state (K^{ss}_{Imax} and K^{ss}_{Imin}) are presented in Fig. 5(a). The half-crack length is a, with a in the interval 1005 μm < a < 1180 μm. Figure 5(b) shows the corresponding values for K_{II}. The coefficient of friction between the crack surfaces was set to 0.5.

As seen from Fig. 5, the magnitude of K_I during the first load cycle was rather insensitive to the crack tip position relative to the interface undulations. The same held for K_{II} both during the first load cycle and at steady state. The exception is $a_i + a_{ii}$ = 1005 μm, which is probably due to the marked change in crack face geometry close to the crack tip for this case. In the interval $a_i < X < a_i + a_{ii}$, a sharp crack tip is modeled, and in the interval $0 < X < a_i$ the geometry of the antibond strip crack is imposed.

K_I attains its largest value during the first loading cycle, and if mode I fracture is assumed to occur as the mode I stress intensity factor reaches the fracture toughness K_{Ic}, the first cycle is the critical one. Thus, the results point toward early crack propagation, which is consistent with the video observations.

At steady state, on the other hand, K_I varies with crack tip position. It can be noted that the crack is open at its tip, at least during parts of the load cycle, for all crack tip positions studied, diminishing the influence of friction.

The results for short cracks are shown in Fig. 6. It is clear that

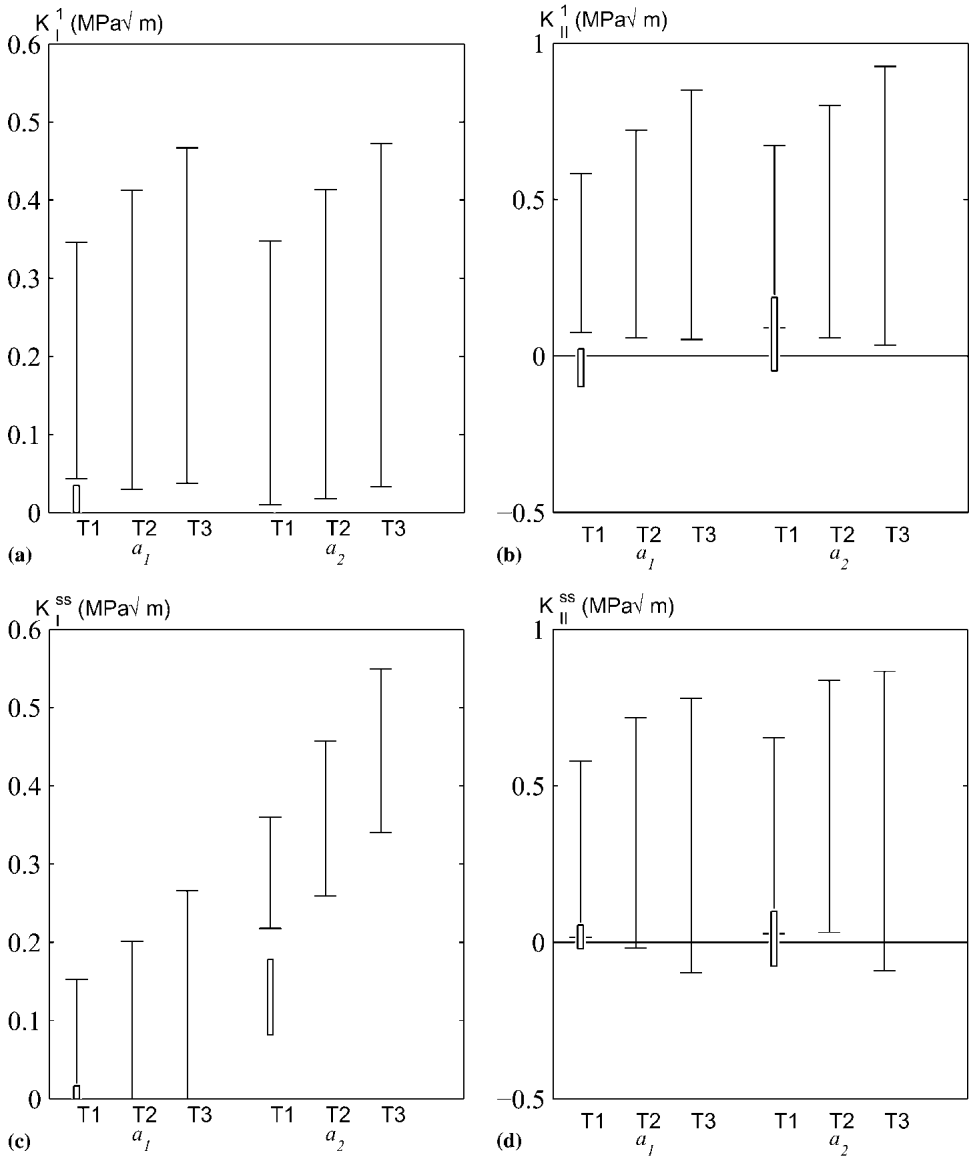

Fig. 7 Magnitude of the stress intensity factor range of (a) K^1_I, (b)K^1_{II}, (c) K^{ss}_I, and (d) K^{ss}_{II}. Solid lines represent antibond cracks of half-crack length a_1 = 1070 μm and a_2 = 1115 μm, and the gray bars represent inherent microcracks of lengths a_1 = 70 μm and a_2 = 115 μm. The friction coefficient between the crack surfaces is 0.5.

for short cracks the stress intensities are low at the first cycle and increase with the number cycles. K_I values are highly dependent on crack position, both during the first cycle and at steady state.

The relative insensitivity to crack tip position relative to the interface undulation for long cracks is expected, because the crack can be regarded as long, which makes the influence from small imperfections less important. The maximum magnitudes of K_I and K_{II} are quite low; K^1_{Imax} is about 0.38 MPa√m, and K^1_{IImax} as well as K^{ss}_{IImax} are about 0.60 MPa√m, regardless of crack length. Assuming mode I fracture and adopting the mode I fracture toughness K_{Ic} = 0.23 MPa√m (Ref 3), mode I fracture occurs already during the first load cycle. If mode I fracture is not initiated during the first cycle, the coating is safe with respect to mode I crack growth at this temperature.

The varying stress state may be one factor contributing to the gradual degradation of the coatings. Other factors are the complex microstructure, with numerous microdefects and with microcracks aligned parallel to the interface. A macrocrack is, thus, not able to propagate freely in the direction of maximum K_I but is guided by the microstructure in preferred directions. The microdefects and the varying stress states constitute possible sites for crack arrest, making a slow gradual degradation possible.

The mode II fracture toughness is generally reported to exceed the mode I fracture toughness by up to one order of magnitude (Ref 7). Because K_{IImax} here only is less than twice K_{Imax}, mode II fracture seems unlikely.

To investigate the influence of maximum temperature on the magnitudes of the stress intensity factors, two different cases were studied. Two different crack lengths were selected: a_1 = 1070 μm, with the crack tip position above a valley of the inter-

face; and a_2 = 1115 μm, with the crack tip position close to an apex. Figure 7(a) to (d) show the variations in magnitude of the stress intensity factors for maximum cycle temperatures $T1$ = 1020 °C, $T2$ = 1140 °C, and $T3$ = 1240 °C as solid lines. Obviously, increasing the temperatures increases all of the stress intensity factor ranges.

To investigate the effect of the crack-face friction on the stress intensity factors, the coefficient of friction was set to zero for all cases corresponding to those in Fig. 7. Influence from friction can be expected only in cases in which the crack is closed over a substantial part of its length during cycling. In line with this reasoning, a marked effect was seen only for the case a_1 = 1070 μm and $T = T3$ = 1240 °C. For this case, the range of K^{ss}_{II} is in the interval $-1.0 < K^{ss}_{II} < 0.8$ MPa√m compared with the range of $-0.1 < K^{ss}_{II} < 0.7$ MPa√m for the case including friction with friction coefficient 0.5. This is an effect of the larger amount of closure for this case compared with the others.

Also included in Fig. 7 are the results assuming a line-formed crack of length a_1 = 70 μm and a_2 = 115 μm, representing inherent microcracks in the as-sprayed samples. The temperature is chosen as T = 930 °C at the top coat surface to account for the temperature drop over the antibond crack and to allow for a comparison between the cases. As seen from Fig. 7, the magnitudes of K_I are much lower for the microcrack compared with the macroscopic crack, as expected.

5. Conclusions

TBC samples, containing microcracks as well as macroscopic cracks on the order of 1 mm, that were subjected to thermal shock loading have been investigated experimentally as well as by FE simulations. The cracks were situated in the top coat close to the interface between the top coat and the bond coat.

As expected, long cracks constitute a larger threat to coating durability compared with short cracks. It was found that macroscopic cracks are prone to rapid initial degradation due to crack extension, a conclusion that is supported by experiments as well as by FE simulations. As-sprayed samples, which are assumed to contain inherent microcracks, degenerate more slowly.

However, both types of samples show a gradual degradation during thermal cycling. The relatively large defect in the antibond strip samples did not lead to an immediate failure in the first few thermal cycles, but the initial rapid degradation seemed to be followed by a slower degradation similar to the degradation of the as-sprayed samples. This is also indicated by the relatively high durability and long life of the antibond samples.

Acknowledgments

The authors thank Robert Dicks, Jonathan Stringer, and Benjamin Russell for their help in performing the thermal shock tests.

References

1. J.T. DeMasi, K.D. Sheffler, and M. Ortiz, "Thermal Barrier Coating Life Prediction Model Development," National Aeronautics and Space Administration Report Cr-182230, NASA-Lewis Research Center, Cleveland, OH, Dec 1989
2. S.M. Meier, D.M. Nilsey, and K.D. Sheffler, "Thermal Barrier Coating Life Prediction Model Development," National Aeronautics and Space Administration Report Cr-189111, NASA-Lewis Research Center, Cleveland, OH, July 1991
3. G. Qian, T. Nakamura, C.C. Berndt, and S.H. Leigh, Tensile Toughness Test and High Temperature Fracture Analysis of Thermal Barrier Coatings, *Acta Mater.,* Vol 45 (No. 4), 1997, p 1767-1784
4. J.T. DeMasi, K.D. Sheffler, and, S. Bose, Mechanisms of Degradation and Failure in a Plasma Deposited Thermal Barrier Coating, *J. Eng. Gas Turbine Power,* Vol 112, 1990, p 521-526
5. D.M. Nissley, Thermal Barrier Coating Life Modelling in Aircraft Gas Turbine Engines, *J. Thermal Spray Technol.,* Vol 6 (No. 1), 1997, p 91-98
6. A.G. Evans, M.Y. He, and J.W. Hutchinson, Effect of Interface Undulations on the Thermal Fatigue of Thin Films and Scales on Metal Substrates, *Acta Mater.,* Vol 45 (No. 9), 1997, p 3543-3554
7. A.G. Evans, D.R. Mumm, J.W. Hutchinson, G.H. Meier, and F.S. Pettit, Mechanisms Controlling the Durability of Thermal Barrier Coatings, *Prog. Mater. Sci.,* Vol 46, 2001, p 505-553
8. Y. Liu, "Life Prediction and Mechanical Behaviour of Thermal Barrier Coatings," Ph.D. dissertation, Lund University, 2003
9. Y. Liu, C. Persson, and J. Wigren, Experimental and Numerical Life Prediction of Thermally Cycled Thermal Barrier Coatings, *J. Thermal Spray Technol.,* Vol 13 (No. 3), 2004, p 415-424
10. Y. Liu, C. Persson, and S. Melin, Numerical Modeling of Short Crack Behavior in Thermal Barrier Coatings upon Thermal Shock Loading, *J. Thermal Spray Technol.,* Vol 13 (No. 3), 2004, p 377-380
11. Hibbitt, Karlsson & Sorensen, Inc., *ABAQUS: User's Manual, Version 6.2*, Hibbitt, Karlsson & Sorensen, Inc., Providence, RI, 2001
12. R.S. Barsoum, On the Use of Isoparametric Finite Elements in Linear Fracture Mechanics, *Int. J. Num. Methods Eng.,* Vol 10, 1976, p 25-37